Macromolecules

pubs.acs.org/Macromolecules Article

Nondestructive Photo-Cross-Linking of Microphase-Separated Diblock Polymers through Coumarin Dimerization

Michael B. Sims, Bo Zhang, Zachary M. Gdowski, Timothy P. Lodge,* and Frank S. Bates*

Cite This: *Macromolecules* 2022, 55, 3317−3324 Read Online

ACCESS | Metrics & More | Article Recommendations | Supporting Information

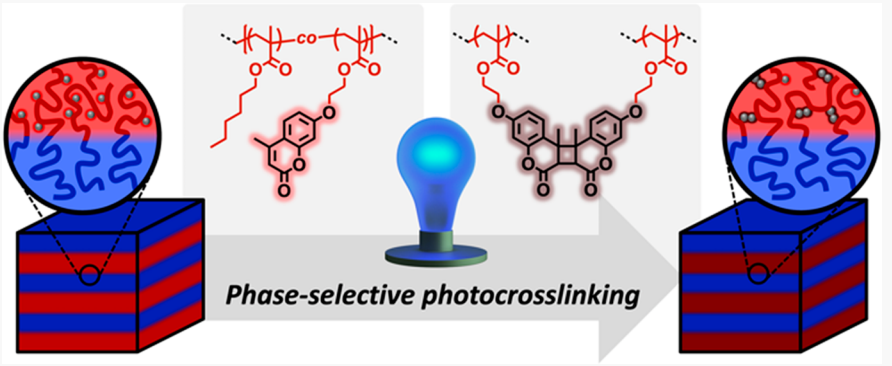

ABSTRACT: The effect of long-wavelength ultraviolet photo-cross-linking on microphase-separated coumarin-containing block polymers was studied by photorheometry and small-angle X-ray scattering. This model system consisted of three photo-cross-linkable diblock polymers of poly(methoxyethyl acrylate)-*b*-poly(hexyl methacrylate-*co*-coumarin methacrylate) with different volume fractions of the cross-linkable coumarin-containing block, which microphase separated into lamellar and cylindrical morphologies. All polymers stiffened upon exposure to 365 nm light, with much greater relative increases in moduli recorded for lamellae-forming polymers (ca. 3200% increase) compared to the cylinder-forming polymer (ca. 550% increase). Disordering transitions that were evident in un-cross-linked samples were no longer observed after cross-linking in the ordered state, and domain sizes were found to remain stable to heating. The photo-cross-linking reaction only proceeded under active irradiation (i.e., cross-linking does not persist when the UV radiation is turned off), indicating a high degree of spatiotemporal control over curing in this system. Finally, at constant concentration of couamarin within the cross-linkable block, the cure rate was largely independent of polymer composition, suggesting a constant local concentration of coumarin moieties within the segregated cross-linkable domains. These findings establish a set of specific structure−property relationships governing the phase-selective photo-cross-linking of diblock polymers that can guide the design of robust nanostructured materials.

INTRODUCTION

Block polymers allow the use of a unique tool—microstructural morphology—for engineering advanced materials, complementing traditional parameters such as molecular weight, structural unit chemistry, and physical interactions.[1] However, ordered states in thermoplastics can be prone to thermal or chemical disruption, upon which the advantageous properties and functions of microstructural order are lost. Phase-selective cross-linking is one strategy for stabilizing potentially delicate microphases, leveraging the exceptional chemical, thermal, and mechanical stability of covalently cross-linked materials. Accordingly, cross-linked block polymers are finding use in advanced materials such as reprocessable thermosets,[2,3] conductive membranes,[4−6] and nanoporous materials.[7−10] Nevertheless, the typical need for exogenous curing agents or elevated curing temperatures may interfere with bottom-up design of specific microstructural features, especially if highly controlled domain sizes or structures that occupy narrow windows of phase space are needed. Curing agents are also often reactive small molecules, and the leaching of these unreacted compounds can pose substantial environmental and health hazards.

Cross-linking via photodimerization of conjugated olefins alleviates many of the aforementioned issues with traditional thermal or chemical curing, as the reaction is highly selective, requires no exogenous reagents, produces no byproducts, and proceeds with acceptable kinetics at room temperature.[11] Olefin photodimerization has been demonstrated with several

Received: February 17, 2022
Revised: March 29, 2022
Published: April 15, 2022

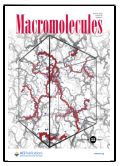

https://doi.org/10.1021/acs.macromol.2c00356
Macromolecules 2022, 55, 3317−3324

Scheme 1. Synthesis of Cross-Linkable Diblock Polymers by ATRP

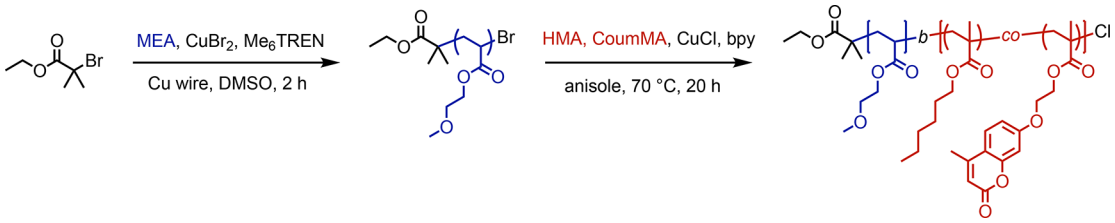

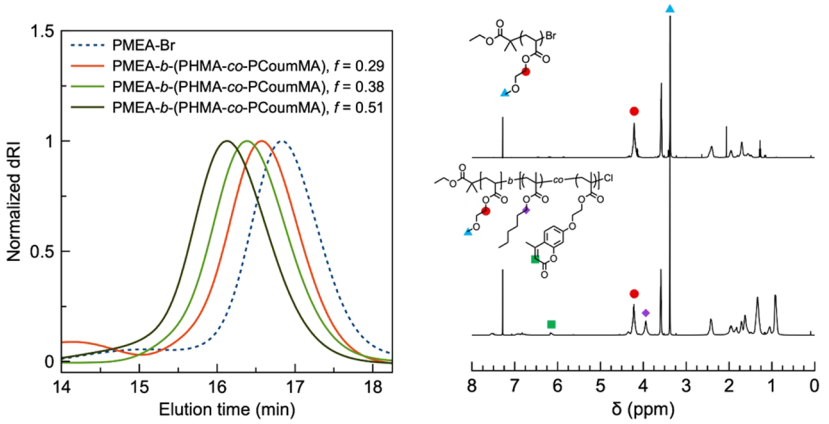

Figure 1. Synthesis of cross-linkable diblock polymers by sequential ATRP (top). Overlaid size-exclusion chromatograms (left) and ^{1}H NMR spectra for diblock polymer with composition $f_{\text{PHMA-}co\text{-PCoumMA}} = 0.51$ (right). Fully annotated and integrated ^{1}H NMR spectra for all polymers can be found in the Supporting Information.

specific moieties (e.g., cinnamic acid derivatives, coumarins, and anthracenes), and all share similar photochemistry—irradiation with the appropriate wavelength of light induces [2 + 2] (or [4 + 4] in the case of anthracene) cycloaddition to yield cyclobutane-linked dimers that undergo cycloreversion upon lower-wavelength light stimulus. Coumarin-containing (co)polymers in particular have drawn considerable attention,[12] largely due to the ease with which coumarin derivatives can be introduced into various polymer structures and the favorable kinetics of their cycloaddition/cycloreversion reactions.[13] In solution, coumarin dimerization has been used for reversible gelation[14−18] and colloidal particle stabilization;[19−23] in bulk materials it has enabled reconfigurable shape-memory materials,[24] 3D-printed soft polyesters,[25] and microphase stabilization.[26,27]

While coumarin-based photochemistry appears highly adaptable to block polymer-based materials, rationally designing such materials requires thoroughly understanding their structure−property relationships, and few studies have examined the interplay between photo-cross-linking, block polymer morphology, and properties. Vana et al. explored the photo-cross-linking of coumarin-containing diblock polymers based on poly(methyl methacrylate)-*b*-poly(butyl acrylate) (PMMA-*b*-PBA), obtaining moderate dimerization efficiencies and modest increases in moduli, presumably due to the localization of coumarin moieties within glassy PMMA domains.[27] Yet there remains a need for a quantitative analysis of how photo-cross-linking impacts ordered morphologies, and vice versa.

We address these specific structure−property relationships in this work by using photorheometry and small-angle X-ray scattering (SAXS) to study the *in situ* photo-cross-linking behavior of three model coumarin-containing diblock polymers that microphase separate into lamellar and cylindrical morphologies. Photorheometry reveals that the cure rate, as measured by increases in the storage modulus (G'), substantially depends on luminous intensity, and the microstructure strongly influences the relative change in modulus upon curing. By performing SAXS on cured samples, we established that curing rendered the polymer microstructure stable to heating beyond the original order−disorder temperature (T_{ODT}) with little change in domain spacing, indicating successful morphological fixation.

RESULTS AND DISCUSSION

Polymer Design and Synthesis. Using sequential ATRP, we synthesized a series of poly(methoxyethyl acrylate)-*b*-poly(hexyl methacrylate-*co*-coumarin methacrylate) (PMEA-*b*-(PHMA-*co*-PCoumMA)) diblock polymers and a control diblock polymer with no coumarin (Scheme 1). ATRP was chosen as the synthetic route due to the inexpensive commercial availability of the materials, wide range of monomers that can be polymerized by using many contemporary variants,[28,29] and relative thermal and photochemical stability of alkyl halide end-groups. The particular synthetic sequence involved first polymerizing MEA through Cu(0)-ATRP with an alkyl bromide initiator[30] followed by chain extension with HMA and CoumMA using a CuCl catalyst. We initially attempted to synthesize an all-acrylate diblock polymer; however, chain extension using coumarin acrylate resulted in a broad and multimodal molecular weight distribution (Figure S1), likely due to cross-linking through the pendent coumarin olefin by reactive acrylate radicals. While this side reaction can produce a macroscopic gel, the system likely remained below the critical gelation conversion and accordingly yielded soluble branched polymers that were amenable to chromatographic analysis.[31] In contrast, using methacrylate derivatives resulted in well-controlled polymer-

https://doi.org/10.1021/acs.macromol.2c00356
Macromolecules 2022, 55, 3317−3324

Table 1. Polymer Characteristics

entry	polymer	$M_{n,SEC}$ (g/mol)[a]	$Đ$	f_B[b]	x_{Coum}[c]	phase[d]
1	PMEA-Br	18100	1.02			
2	PMEA-*b*-PHMA	34200	1.12	0.47		
3 (**DB29$_{0.19}$**)	PMEA-*b*-(PHMA-*co*-PCoumMA)	25300	1.06	0.29	0.19	HEX
4 (**DB38$_{0.18}$**)	PMEA-*b*-(PHMA-*co*-PCoumMA)	29000	1.03	0.38	0.18	LAM
5 (**DB47$_{0.10}$**)	PMEA-*b*-(PHMA-*co*-PCoumMA)	34400	1.10	0.47	0.10	LAM
6 (**DB51$_{0.21}$**)	PMEA-*b*-(PHMA-*co*-PCoumMA)	35800	1.03	0.51	0.21	LAM

[a]Determined from SEC-MALS. [b]Volume fraction of PHMA-*co*-PCoumMA block, where densities were determined from the literature values for PMEA (ρ = 1.09 g/mL) and PHMA (ρ = 1.01 g/mL) and from group contribution theory[33] for PCoumMA (ρ = 1.23 g/mL). [c]Mole fraction of CoumMA structural units within the PHMA-*co*-PCoumMA block determined from ^{1}H NMR spectroscopy. [d]Determined from SAXS.

ization and coumarin preservation (Figure 1, Figure S2, and Figure S3) by virtue of the lower ground-state energies of the methacrylate radicals. To achieve good control over the chain extension of a bromide-terminated polyacrylate with a polymethacrylate block, an *in situ* halogen exchange reaction was employed to appropriately balance initiation and propagation kinetics.[32] Finally, we characterized the relative rates of comonomer enchainment in a copolymerization with 10 mol % CoumMA, finding that CoumMA is incorporated substantially faster than HMA (Figure S4). After 1 h of reaction, CoumMA reached 90% conversion whereas HMA reached 51% conversion, suggesting gradient copolymerization behavior. Nevertheless, the associated tapering of CoumMA did not interfere with microphase separation or radiation-induced curing.

This macromolecular design targeted three necessary properties for this study: an accessible order−disorder transition temperature (T_{ODT}), moderate degrees of polymerization (N) to yield practical ordering/disordering kinetics, and a low glass transition temperature (T_g) to extend the temperature range over which ordering/disordering and effective cross-linking could be performed. Achieving the first two properties required selecting two blocks with sufficient segregation strength (as exemplified by the Flory−Huggins interaction parameter, χ), which was accomplished through the pairing of a polar acrylic block with a nonpolar methacrylic block. To assess the impact of polymer microstructure on both the coumarin-based curing reaction and resultant material properties, we synthesized a series of diblock polymers spanning cross-linkable block volume fractions (f_B) of 0.29−0.51 and varying mole fractions of coumarin (x_{Coum}) within the cross-linkable blocks, which formed cylindrical (HEX) and lamellar (LAM) microstructures in the ordered state (Table 1).

Polymer Characterization. Differential scanning calorimetry (DSC) of **DB51$_{0.21}$** revealed two T_gs: a sharp transition at −30 °C that corresponds to the PMEA block and a broad transition centered at 28 °C that corresponds to the PHMA-*co*-PCoumMA block (Figure S5). The second block exhibits a higher T_g than PHMA homopolymer (−5 °C), as the rigid PCoumMA units are expected to increase the glassiness of the statistical copolymer with increasing CoumMA incorporation.

The microstructures of each diblock polymer were characterized using a lab-source SAXS instrument (Figure 2). **DB51$_{0.21}$** and **DB38$_{0.18}$** each exhibit sharp principal scattering peaks at q^* = 0.0283 Å^{-1} and q^* = 0.0317 Å^{-1} ($q = 4\pi\lambda^{-1}\sin(\theta/2)$ where λ = 1.54 Å is the radiation wavelength and θ is the scattering angle), indicating strongly segregated microstructures with domain spacings d = 22.3 and 19.8 nm, respectively, where $d = 2\pi/q^*$. The presence of multiple integer-spaced higher-order reflections further confirms

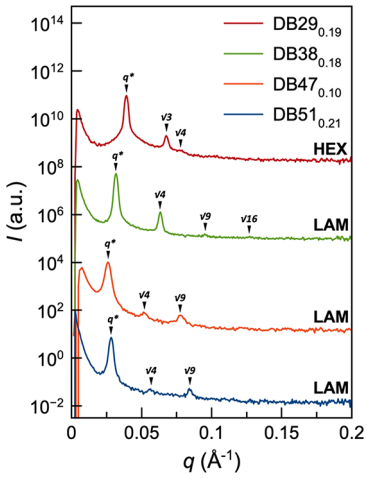

Figure 2. Small-angle X-ray scattering patterns obtained for polymers **DB29$_{0.19}$** (green trace), **DB38$_{0.18}$** (green trace), and **DB51$_{0.21}$** (maroon trace) at 50 °C and for **DB47$_{0.10}$** (orange trace) at 25 °C. Polymers were annealed at 50 °C for 18 h prior to measurement. LAM and HEX refer to lamellar and hexagonally ordered cylindrical microdomains.

lamellar morphologies, and in **DB51$_{0.21}$**, suppression of the $\sqrt{4}$ reflection is consistent with structure factor extinction in compositionally symmetric lamellae. **DB29$_{0.19}$** exhibits a broader q^* peak at q = 0.0392 Å^{-1} (d = 16.0 nm) and reflections at $\sqrt{3}$ and $\sqrt{4}$, indicating hexagonally packed cylinders. Using temperature-controlled SAXS, we determined approximate disordering temperatures for **DB51$_{0.21}$**, **DB38$_{0.18}$**, and **DB29$_{0.19}$** (Figure S6). **DB51$_{0.21}$** remained ordered over the entire temperature range scanned, implying a T_{ODT} > 200 °C. Disordering occurred between 170 and 210 °C for **DB38$_{0.18}$** and between 60 and 90 °C for **DB29$_{0.19}$**. We elected to conduct detailed cross-linking studies on **DB38$_{0.18}$** and **DB29$_{0.19}$** due to the accessible ODT temperatures.

Lamellar Phase Cross-Linking. Prior to cross-linking, the viscoelastic properties of **DB38$_{0.18}$** were characterized by oscillatory shear rheometry (Figure S7). Frequency sweep experiments revealed a scaling relationship of $G' \approx G'' \sim \omega^{0.42}$ at low frequencies, which is close to the established behavior exhibited by symmetric, ordered diblock polymers ($G' \approx G'' \sim \omega^{0.50}$).[34] Furthermore, temperature ramps from 55 to 120 °C show close coupling between G' and G'' with no evidence of disordering (which would be reflected as a crossover to liquid-like terminal behavior). We then performed photorheometry to monitor the curing of **DB38$_{0.18}$** in real time by subjecting the polymer to continuous oscillatory shear (strain amplitude of 0.5%) while irradiating the specimen with 365 nm light delivered through a quartz window that serves as the lower

https://doi.org/10.1021/acs.macromol.2c00356
Macromolecules 2022, 55, 3317−3324

portion of the parallel plate fixture. The polymer was first conditioned at 50 °C for 2 h to ensure full thermal equilibration, and then irradiation was begun after a 5 min delay to record the initial modulus. Both G' and G'' began increasing immediately after irradiation commenced and had nearly plateaued after 10 h, resulting in substantial stiffening from G' = 10.5 kPa to G' = 350 kPa (Figure 3). Because the *in*

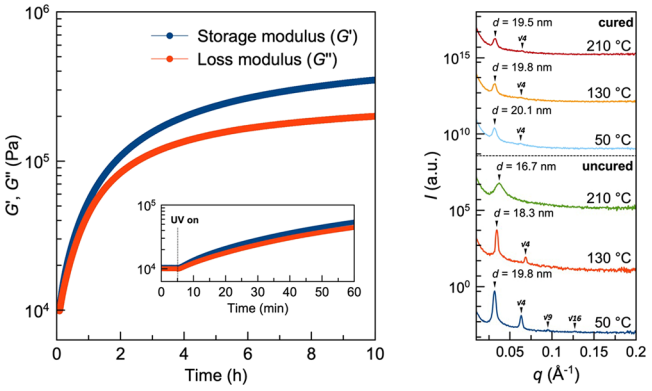

Figure 3. Oscillatory shear rheometry of $\mathbf{DB38}_{0.18}$ at 50 °C under illumination with 365 nm light (conditions: strain = 0.5%, frequency = 1.0 rad/s, light intensity = 51.2 mW/cm^2, sample thickness = 500 μm, anneal time = 2 h) (left). Small-angle X-ray scattering patterns of $\mathbf{DB38}_{0.18}$ at 50, 130, and 210 °C before curing and after curing for 10 h (right).

situ rheological properties were obtained in the linear viscoelastic regime (see Figure S7), we do not believe that the small-amplitude strain influences the cross-linking kinetics. When $\mathbf{DB51}_{0.21}$ was cross-linked in the same manner at 50 °C, G' increased from 68 kPa to 2.2 MPa (Figure S8). The same procedure was performed on a near-symmetric PMEA-*b*-PHMA diblock polymer containing no coumarin (entry **2**, Table 1) and yielded no change in moduli other than small decreases presumably from radiant heating (Figure S9), implying that coumarin dimerization is the sole cross-linking mechanism in this system.

SAXS patterns of a cured sample indicated that cross-linking had stabilized the lamellar microstructure. Prior to curing, $\mathbf{DB38}_{0.18}$ exhibited both a disordering transition between 170 and 210 °C and a contraction of domain spacing (d) from 19.8 to 16.7 nm, as indicated by the progressive shift in q^* toward higher q-values as temperature increased. This decrease in d arises from greater mixing of A- and B-blocks due to reduced segregating power, in turn leading to increased interfacial thickness, reduced chain stretching, and smaller interlamellar spacings.[35] After curing, an ordered lamellar morphology persisted up to 210 °C, and the presence of a $\sqrt{4}$ peak at all temperatures suggests that longer-range order is substantially retained. The domain spacing was also rendered thermally stable after cross-linking, with d remaining relatively constant over the temperature range of 50−210 °C for the cured sample compared to a 16% contraction for the uncured sample. Finally, moderate peak broadening was observed after cross-linking, which is likely a consequence of domains being slightly perturbed from a thermodynamically stable state after cross-linking. Regions with locally lower cross-link densities would be better able to relax to the new equilibrium domain size, which would manifest as a broader domain size distribution.

Coumarin dimerization proceeds through the formation of a photoexcited state;[36] therefore, higher luminous intensity is expected to accelerate curing by increasing the concentration of photoexcited coumarin molecules. Consistent with this expectation, we increased the light intensity from 22.2 to 106 mW/cm^2 and obtained progressively faster curing with no evidence of degradation, even at the highest intensity (Figure 4). A previous study of coumarin-cross-linked polycarbonates

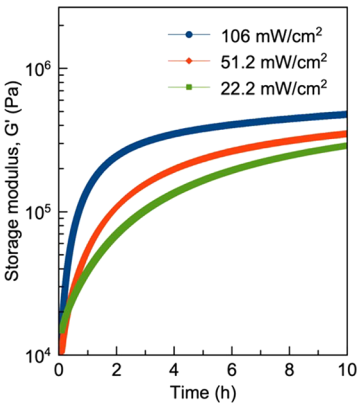

Figure 4. Oscillatory shear rheometry of $\mathbf{DB38}_{0.18}$ under illumination with 365 nm light at intensities of 106 mW/cm^2 (blue trace), 51.2 mW/cm^2 (orange trace), and 22.2 mW/cm^2 (green trace) (conditions: strain = 0.5%, frequency = 1.0 rad/s, temperature = 50 °C, anneal time = 2 h).

found evidence of network degradation when UV intensities between 700 and 1400 mW/cm^2 were used,[37] suggesting there is a practical upper limit to enhancing the cure rate via intensity. We additionally examined the effect of sample thickness on cure rate, anticipating that thicker samples would cure more slowly, but there was no discernible difference in a 500 μm sample versus a 250 μm sample (Figure S10). Ultraviolet−visible spectroscopy of a 100 μm thick film of $\mathbf{DB38}_{0.18}$ found an absorbance value of 0.075 at 365 nm, indicating 65% transmittance for a 250 μm sample and 42% transmittance for a 500 μm sample. This relatively small difference in transmittance, along with the fact that the material becomes more UV-transparent as it cures, leads to the conclusion that observable differences in the thickness-dependent cure rate would only manifest in samples with substantially different thicknesses or reduced transparency.

Light irradiation can be performed with a high degree of spatial and temporal specificity, enabling precise control over the modification of photochemically active materials.[38] To determine the extent to which we could assert this control over these coumarin-containing materials, we performed a step-cure experiment in which the modulus of the sample was monitored while the UV light was cycled on and off (Figure 5). G' and G'' progressively increased while the light was on, and curing almost entirely ceased as soon as the light was turned off (the small step changes in moduli between cycles are believed to arise from radiant heating of less than 0.5 °C based on temperature ramp data). This behavior is clear evidence that cross-linking proceeds via the formation of cyclobutane-linked coumarin dimers, a mechanism that has been thoroughly established with small molecule and polymeric systems.[11]

Hexagonal Phase Cross-Linking. Having demonstrated that coumarin-based photo-cross-linking can efficiently cure and stabilize a lamellar diblock polymer, the next objective was

https://doi.org/10.1021/acs.macromol.2c00356
Macromolecules 2022, 55, 3317−3324

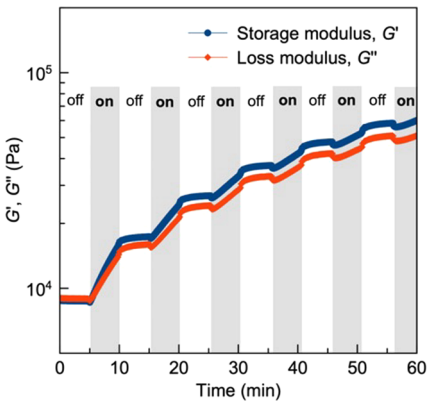

Figure 5. Step-curing of $\mathbf{DB38}_{0.18}$ at 50 °C in which the UV light shutter was sequentially opened and closed in 5 min intervals, demonstrating that curing occurs only under active irradiation (conditions: strain = 0.5%, frequency = 1.0 rad/s, light intensity = 106 mW/cm^2, sample thickness = 500 μm, anneal time = 2 h).

to determine the effect of microstructural morphology on the cure behavior and resultant material properties. As with the previous polymer, we characterized the viscoelastic properties of $\mathbf{DB29}_{0.19}$ prior to curing by oscillatory shear rheometry. The frequency sweep depicts a pattern characteristic of cylindrical diblock polymers,[34] (Figure S11), and the temperature scan from 60 to 90 °C depicts a transition from viscoelastic solid to fluid at 76 °C (Figure 6). While this transition does not display the classical appearance of an ODT (i.e., step change in elastic modulus), a frequency sweep at 90 °C revealed approximately terminal behavior (Figure S12) indicative of a disordered state; Figure 2 confirms ordered cylinders at 50 °C.

$\mathbf{DB29}_{0.19}$ was cured analogously to $\mathbf{DB38}_{0.18}$, and qualitatively similar cure kinetics were obtained: a rapid initial increase in modulus for the first 1−2 h of cure time, followed by a much slower increase in modulus for the remainder of the experiment (Figure 6). This similarity is unsurprising, as the molar concentrations of coumarin moieties within the ordered domains of both polymers are nearly identical despite the different morphologies. A temperature scan after cross-linking in the ordered state reveals persistent solid-like behavior with no evidence of a disordering transition between 55 and 120 °C, consistent with the presence of a disordered network of cross-linked cylinders throughout the material. This finding is in accordance with recent work by Xu et al., who found that grain defects in unaligned HEX-forming polymers enabled sufficient percolation of the cylindrical phase to yield rigid networks after cross-linking.[39]

SAXS analysis further corroborates the conclusions drawn from the rheological data (Figure 7). An uncured sample of

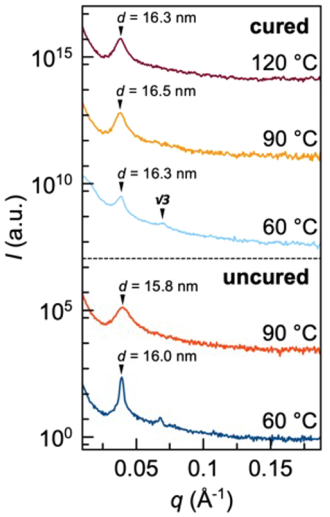

Figure 7. Small-angle X-ray scattering patterns of $\mathbf{DB29}_{0.19}$ before and after curing. A clear order−disorder transition occurs between 60 and 90 °C in the uncured sample.

$\mathbf{DB29}_{0.19}$ underwent disordering between 60 and 90 °C; however, after curing the shape and position of q^* did not change (although the $\sqrt{3}$ peak disappeared). The cylindrical domain size was also resistant to change upon heating, with virtually no change in d recorded upon heating from 60 to 120 °C. As with $\mathbf{DB38}_{0.18}$, slight broadening of q^* was obtained after curing, likely due to distortion of the microdomain structure by local stresses associated with cross-linking.

Disordered State Cross-Linking. As a final point of morphological comparison, we cross-linked $\mathbf{DB29}_{0.19}$ in the disordered state ($\mathbf{DB29}_{0.19}$-**DIS**) at 90 °C (Figure 8). Because of the fluid-like nature of this material, it was possible to observe a crossover indicating macroscopic gelation after 37

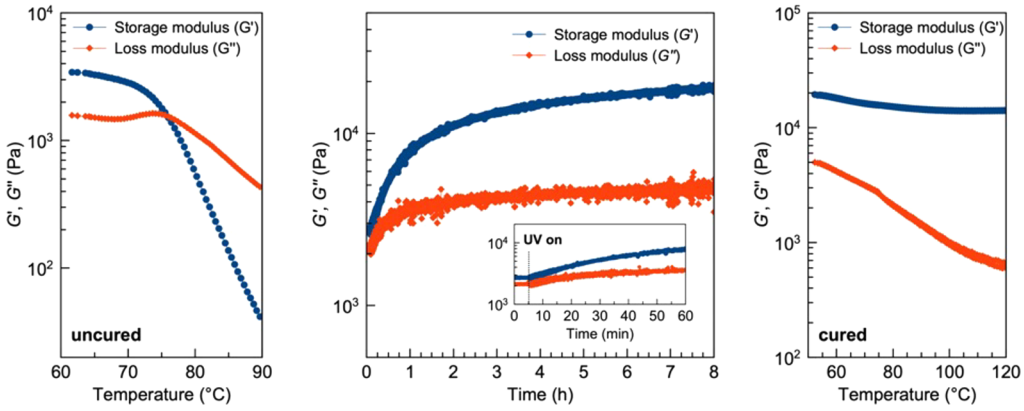

Figure 6. Temperature ramp of $\mathbf{DB29}_{0.19}$ prior to curing depicting a crossover to viscoelastic fluid behavior at 76 °C (left). Curing kinetics of $\mathbf{DB29}_{0.19}$ at 60 °C under a luminous intensity of 106 mW/cm^2 (middle). Temperature ramp of $\mathbf{DB29}_{0.19}$ immediately after curing with no crossover between G' and G'' (conditions: strain = 0.5%, frequency = 1.0 rad/s, light intensity = 106 mW/cm^2, sample thickness = 500 μm, anneal time = 2 h) (right).

https://doi.org/10.1021/acs.macromol.2c00356
Macromolecules 2022, 55, 3317−3324

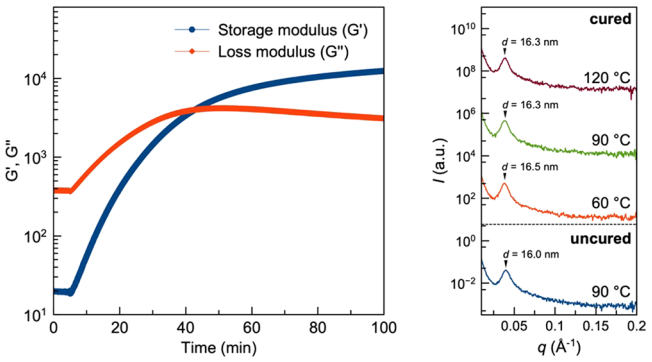

Figure 8. Oscillatory shear rheometry of **DB29$_{0.19}$** at 90 °C depicting a crossover at 43 min (38 min of cure time) (conditions: strain = 1.0%, frequency = 1.0 rad/s, light intensity = 106 mW/cm^2, sample thickness = 500 μm, anneal time = 2 h) (left). Small-angle X-ray scattering patterns before and after curing **DB29$_{0.19}$** at 90 °C (right).

min of curing. SAXS patterns after curing also show a broad q^* peak centered at q = 0.038 Å^{-1} (d = 16.5 nm) that exhibits little change in shape, position, or intensity upon heating, which is consistent with a disorganized network structure. Interestingly, **DB29$_{0.19}$** and **DB29$_{0.19}$-DIS** approach similar asymptotic moduli despite being of formally different microstructures. It is likely that by cross-linking **DB29$_{0.19}$-DIS** in such proximity to the ODT, a fluctuating disordered state that approximates the weakly ordered cylindrical state of **DB29$_{0.19}$** at 60 °C is captured. This hypothesis additionally explains why **DB29$_{0.19}$** and **DB29$_{0.19}$-DIS** exhibit similar SAXS patterns and domain spacings after curing despite being cured in different states of microstructural order.

When directly comparing the curing of lamellae- and cylinder-forming polymers as storage modulus normalized to the initial value (G'/G'_0) (Figure 9), the influence of

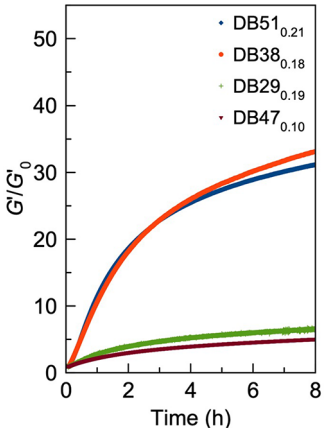

Figure 9. Relative increases in G′ for **DB51$_{0.21}$** (blue trace), **DB38$_{0.18}$** (orange trace), **DB29$_{0.19}$** (green trace), and **DB47$_{0.10}$** (maroon trace) normalized to G′ at 0 h (G′$_0$).

microstructure becomes strikingly apparent: G'_{DB51} increased from 68 kPa to 2.2 MPa (31-fold increase) and G'_{DB38} increased from 13 to 480 kPa (33-fold increase), whereas G'_{DB29} increased from 2.7 to 10 kPa (4-fold increase). In fact, microstructural effects in this system are so substantial that the curing behavior of **DB29$_{0.19}$** is on par with that of **DB47$_{0.10}$**, even though the former contains twice the coumarin concentration in the cross-linkable block. This disparate stiffening behavior is likely a consequence of the different connectivity of lamellar and cylindrical domains at grain boundaries. There are more orientations in which 2-dimensional lamellar sheets may connect at grain boundaries to produce a percolating network compared to 1-dimensional cylinders, which produces a denser network of elastically effective cross-linked domains. Further supporting evidence for the unique role of microstructure—as opposed to merely differences in f_B—comes from the fact that the lamellar polymers **DB51** and **DB38$_{0.18}$** exhibit similar relative modulus increases, despite differing in f_B by a greater amount than **DB38$_{0.18}$** and **DB29$_{0.19}$**.

When comparing the rates of modulus increase of **DB51$_{0.21}$**, **DB47$_{0.10}$**, **DB38$_{0.18}$**, and **DB29$_{0.19}$**, the curing kinetics are remarkably independent of the total coumarin concentration in the diblock polymer, instead appearing to correlate with the coumarin concentration solely within the cross-linkable block (x_{CoumMA}) (Figure 10). The highest cure rate is exhibited by

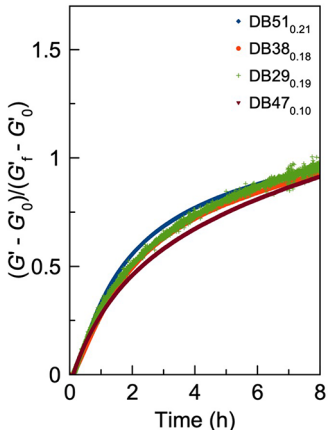

Figure 10. Curing kinetics for **DB51$_{0.21}$** (blue trace), **DB38$_{0.18}$** (orange trace), **DB29$_{0.19}$** (green trace), and **DB47$_{0.10}$** (maroon trace) depicted as relative increase in modulus, normalized to the change in G′ after 8 h of curing (G′$_f$ − G′$_0$).

DB51$_{0.21}$, and it progressively decreased as x_{CoumMA} decreased. We believe this behavior occurs in states of strong or intermediate segregation, where the PMEA block is largely excluded from PHMA-*co*-PCoumMA domains. As a result, the overall curing kinetics are governed by the local concentration of cross-linkable PCoumMA structural units within PCoumMA-rich domains, rather than by f_B or the global cross-linker concentration.

CONCLUSIONS

We have leveraged an efficient synthesis of coumarin-containing diblock polymers to design a series of microphase-separated materials in which the minority phase could be selectively cross-linked under UV light irradiation. Using a combination of photorheometry and SAXS, we studied the relationship between block polymer microstructure and curing behavior in detail, finding that coumarin dimerization enables fixation of both the morphology and its dimensions without requiring exogenous reagents or producing byproducts. The cure rate appears to predominantly depend on the concentration of coumarin within the cross-linkable domain, as similar rates were observed for all microstructures. However, the relative change in modulus upon curing strongly depends on

https://doi.org/10.1021/acs.macromol.2c00356
Macromolecules 2022, 55, 3317−3324

the microstructure, with more highly percolating phases yielding stiffer networks. These findings establish design principles for cross-linkable microphase-separated materials, which should be valuable in developing nanostructured materials with tailored mechanical properties.

■ ASSOCIATED CONTENT

Supporting Information

The Supporting Information is available free of charge at https://pubs.acs.org/doi/10.1021/acs.macromol.2c00356.

Instrumental details, synthetic procedures, and complete characterization data (PDF)

■ AUTHOR INFORMATION

Corresponding Authors

Timothy P. Lodge − *Department of Chemical Engineering and Materials Science and Department of Chemistry, University of Minnesota, Minneapolis, Minnesota 55455, United States;* orcid.org/0000-0001-5916-8834; Email: lodge@umn.edu

Frank S. Bates − *Department of Chemical Engineering and Materials Science, University of Minnesota, Minneapolis, Minnesota 55455, United States;* orcid.org/0000-0003-3977-1278; Email: bates001@umn.edu

Authors

Michael B. Sims − *Department of Chemical Engineering and Materials Science, University of Minnesota, Minneapolis, Minnesota 55455, United States;* orcid.org/0000-0002-5308-3386

Bo Zhang − *Department of Chemical Engineering and Materials Science, University of Minnesota, Minneapolis, Minnesota 55455, United States;* orcid.org/0000-0001-5366-1855

Zachary M. Gdowski − *Department of Chemical Engineering and Materials Science, University of Minnesota, Minneapolis, Minnesota 55455, United States*

Complete contact information is available at: https://pubs.acs.org/10.1021/acs.macromol.2c00356

Notes

The authors declare no competing financial interest.

■ ACKNOWLEDGMENTS

This work was supported by the Office of Basic Energy Sciences (BES) of the U.S. Department of Energy (DoE) under Contract DE-SC0017809. SAXS was performed at the University of Minnesota Characterization Facility, which receives partial support from the National Science Foundation MRSEC program (DMR-2011401).

■ REFERENCES

(1) Bates, C. M.; Bates, F. S. 50th Anniversary Perspective: Block Polymers—Pure Potential. *Macromolecules* **2017**, *50*, 3−22.

(2) Lessard, J. J.; Scheutz, G. M.; Sung, S. H.; Lantz, K. A.; Epps, T. H.; Sumerlin, B. S. Block Copolymer Vitrimers. *J. Am. Chem. Soc.* **2020**, *142*, 283−289.

(3) Ishibashi, J. S. A.; Pierce, I. C.; Chang, A. B.; Zografos, A.; El-Zaatari, B. M.; Fang, Y.; Weigand, S. J.; Bates, F. S.; Kalow, J. A. Mechanical and Structural Consequences of Associative Dynamic Cross-Linking in Acrylic Diblock Copolymers. *Macromolecules* **2021**, *54*, 3972−3986.

(4) Schulze, M. W.; McIntosh, L. D.; Hillmyer, M. A.; Lodge, T. P. High-Modulus, High-Conductivity Nanostructured Polymer Electrolyte Membranes via Polymerization-Induced Phase Separation. *Nano Lett.* **2014**, *14*, 122−126.

(5) Chopade, S. A.; So, S.; Hillmyer, M. A.; Lodge, T. P. Anhydrous Proton Conducting Polymer Electrolyte Membranes via Polymerization-Induced Microphase Separation. *ACS Appl. Mater. Interfaces* **2016**, *8*, 6200−6210.

(6) Chopade, S. A.; Au, J. G.; Li, Z.; Schmidt, P. W.; Hillmyer, M. A.; Lodge, T. P. Robust Polymer Electrolyte Membranes with High Ambient-Temperature Lithium-Ion Conductivity via Polymerization-Induced Microphase Separation. *ACS Appl. Mater. Interfaces* **2017**, *9*, 14561−14565.

(7) Vidil, T.; Hampu, N.; Hillmyer, M. A. Nanoporous Thermosets with Percolating Pores from Block Polymers Chemically Fixed above the Order−Disorder Transition. *ACS Central Science* **2017**, *3*, 1114−1120.

(8) Zhou, N.; Bates, F. S.; Lodge, T. P. Mesoporous Membrane Templated by a Polymeric Bicontinuous Microemulsion. *Nano Lett.* **2006**, *6*, 2354−2357.

(9) Hillmyer, M. A.; Lipic, P. M.; Hajduk, D. A.; Almdal, K.; Bates, F. S. Self-Assembly and Polymerization of Epoxy Resin-Amphiphilic Block Copolymer Nanocomposites. *J. Am. Chem. Soc.* **1997**, *119*, 2749−2750.

(10) Seo, M.; Hillmyer, M. A. Reticulated Nanoporous Polymers by Controlled Polymerization-Induced Microphase Separation. *Science* **2012**, *336*, 1422−1425.

(11) Kaur, G.; Johnston, P.; Saito, K. Photo-reversible dimerisation reactions and their applications in polymeric systems. *Polym. Chem.* **2014**, *5*, 2171−2186.

(12) Trenor, S. R.; Shultz, A. R.; Love, B. J.; Long, T. E. Coumarins in Polymers: From Light Harvesting to Photo-Cross-Linkable Tissue Scaffolds. *Chem. Rev.* **2004**, *104*, 3059−3078.

(13) Chen, Y.; Chou, C.-F. Reversible photodimerization of coumarin derivatives dispersed in poly(vinyl acetate). *J. Polym. Sci., Part A: Polym. Chem.* **1995**, *33*, 2705−2714.

(14) Kabb, C. P.; O'Bryan, C. S.; Deng, C. C.; Angelini, T. E.; Sumerlin, B. S. Photoreversible Covalent Hydrogels for Soft-Matter Additive Manufacturing. *ACS Appl. Mater. Interfaces* **2018**, *10*, 16793−16801.

(15) Azagarsamy, M. A.; McKinnon, D. D.; Alge, D. L.; Anseth, K. S. Coumarin-Based Photodegradable Hydrogel: Design, Synthesis, Gelation, and Degradation Kinetics. *ACS Macro Lett.* **2014**, *3*, 515−519.

(16) Nagata, M.; Yamamoto, Y. Photoreversible poly(ethylene glycol)s with pendent coumarin group and their hydrogels. *React. Funct. Polym.* **2008**, *68*, 915−921.

(17) Zhu, C. N.; Li, C. Y.; Wang, H.; Hong, W.; Huang, F.; Zheng, Q.; Wu, Z. L. Reconstructable Gradient Structures and Reprogrammable 3D Deformations of Hydrogels with Coumarin Units as the Photolabile Crosslinks. *Adv. Mater.* **2021**, *33*, 2008057.

(18) Wang, L.; Ma, X.; Wu, L.; Sha, Y.; Yu, B.; Lan, X.; Luo, Y.; Shi, Y.; Wang, Y.; Luo, Z. Coumarin derivative trigger controlled photo-healing of ion gels and photo-controlled reversible adhesiveness. *Eur. Polym. J.* **2021**, *144*, 110213.

(19) Jiang, J.; Qi, B.; Lepage, M.; Zhao, Y. Polymer Micelles Stabilization on Demand through Reversible Photo-Cross-Linking. *Macromolecules* **2007**, *40*, 790−792.

(20) He, J.; Zhao, Y. Light-responsive polymer micelles, nano- and microgels based on the reversible photodimerization of coumarin. *Dyes Pigm.* **2011**, *89*, 278−283.

(21) He, J.; Tong, X.; Tremblay, L.; Zhao, Y. Corona-Cross-Linked Polymer Vesicles Displaying a Large and Reversible Temperature-Responsive Volume Transition. *Macromolecules* **2009**, *42*, 7267−7270.

(22) He, J.; Tremblay, L.; Lacelle, S.; Zhao, Y. Preparation of polymer single chain nanoparticles using intramolecular photodimerization of coumarin. *Soft Matter* **2011**, *7*, 2380−2386.

(23) Scheutz, G. M.; Elgoyhen, J.; Bentz, K. C.; Xia, Y.; Sun, H.; Zhao, J.; Savin, D. A.; Sumerlin, B. S. Mediating covalent crosslinking

of single-chain nanoparticles through solvophobicity in organic solvents. *Polym. Chem.* **2021**, *12*, 4462−4466.
(24) Defize, T.; Thomassin, J.-M.; Ottevaere, H.; Malherbe, C.; Eppe, G.; Jellali, R.; Alexandre, M.; Jérôme, C.; Riva, R. Photo-Cross-Linkable Coumarin-Based Poly(ε-caprolactone) for Light-Controlled Design and Reconfiguration of Shape-Memory Polymer Networks. *Macromolecules* **2019**, *52*, 444−456.
(25) Govindarajan, S. R.; Xu, Y.; Swanson, J. P.; Jain, T.; Lu, Y.; Choi, J.-W.; Joy, A. A Solvent and Initiator Free, Low-Modulus, Degradable Polyester Platform with Modular Functionality for Ambient-Temperature 3D Printing. *Macromolecules* **2016**, *49*, 2429−2437.
(26) Xue, B.; Li, X.; Gao, L.; Gao, M.; Wang, Y.; Jiang, L. CO_2-selective free-standing membrane by self-assembly of a UV-cross-linkable diblock copolymer. *J. Mater. Chem.* **2012**, *22*, 10918−10923.
(27) Tietz, K.; Finkhäuser, S.; Samwer, K.; Vana, P. Stabilizing the Microphase Separation of Block Copolymers by Controlled Photo-crosslinking. *Macromol. Chem. Phys.* **2014**, *215*, 1563−1572.
(28) Matyjaszewski, K. Atom Transfer Radical Polymerization (ATRP): Current Status and Future Perspectives. *Macromolecules* **2012**, *45*, 4015−4039.
(29) Truong, N. P.; Jones, G. R.; Bradford, K. G. E.; Konkolewicz, D.; Anastasaki, A. A comparison of RAFT and ATRP methods for controlled radical polymerization. *Nat. Rev. Chem.* **2021**, *5*, 859−869.
(30) Anastasaki, A.; Waldron, C.; Wilson, P.; Boyer, C.; Zetterlund, P. B.; Whittaker, M. R.; Haddleton, D. High Molecular Weight Block Copolymers by Sequential Monomer Addition via Cu(0)-Mediated Living Radical Polymerization (SET-LRP): An Optimized Approach. *ACS Macro Lett.* **2013**, *2*, 896−900.
(31) Sims, M. B. Controlled radical copolymerization of multivinyl crosslinkers: a robust route to functional branched macromolecules. *Polym. Int.* **2021**, *70*, 14−23.
(32) Shipp, D. A.; Wang, J.-L.; Matyjaszewski, K. Synthesis of Acrylate and Methacrylate Block Copolymers Using Atom Transfer Radical Polymerization. *Macromolecules* **1998**, *31*, 8005−8008.
(33) Van Krevelen, D. W.; Hoftyzer, P. J. Prediction of polymer densities. *J. Appl. Polym. Sci.* **1969**, *13*, 871−881.
(34) Fredrickson, G. H.; Bates, F. S. Dynamics of Block Copolymers: Theory and Experiment. *Annu. Rev. Mater. Sci.* **1996**, *26*, 501−550.
(35) Hashimoto, T.; Shibayama, M.; Kawai, H. Ordered structure in block polymer solutions. 4. Scaling rules on size of fluctuations with block molecular weight, concentration, and temperature in segregation and homogeneous regimes. *Macromolecules* **1983**, *16*, 1093−1101.
(36) Hammond, G. S.; Stout, C. A.; Lamola, A. A. Mechanisms of Photochemical Reactions in Solution. XXV. The Photodimerization of Coumarin. *J. Am. Chem. Soc.* **1964**, *86*, 3103−3106.
(37) Chesterman, J. P.; Hughes, T. C.; Amsden, B. G. Reversibly photo-crosslinkable aliphatic polycarbonates functionalized with coumarin. *Eur. Polym. J.* **2018**, *105*, 186−193.
(38) Hui, E.; Gimeno, K. I.; Guan, G.; Caliari, S. R. Spatiotemporal Control of Viscoelasticity in Phototunable Hyaluronic Acid Hydrogels. *Biomacromolecules* **2019**, *20*, 4126−4134.
(39) Xu, H.; Xiao, H.; Ellison, C. J.; Mahanthappa, M. K. Flexible Nanoporous Materials by Matrix Removal from Cylinder-Forming Diblock Copolymers. *Nano Lett.* **2021**, *21*, 7587−7594.

https://doi.org/10.1021/acs.macromol.2c00356
Macromolecules 2022, 55, 3317−3324